Cent. Eur. J. Geosci. • 1(2) • 2011 • 155-168
DOI: 10.2478/s13533-011-0012-8

Springer

Central European Journal of **Geosciences**

Hypogeal geological survey in the ”Grotta del Re Tiberio” natural cave (Apennines, Italy): a valid tool for reconstructing the structural setting

Research Article

Alice Ghiselli[1]*, Marzio Merazzi[1], Andrea Strini[1], Roberto Margutti[2], Michele Mercuriali[2]

1 *Studio Associato GSM, Geo and Speleo Matters cons.- Milano, 20132, via Rizzoli, 49, Italy*

2 *Saint-Gobain PPC Italia S.p.A., Dip.t “Exploration, Mining & Recycling” - Milano, 20145, via Ettore Romagnoli, 6, Italy*

Received 23 November 2010; accepted 9 March 2011

Abstract: As karst systems are natural windows to the underground, speleology, combined with geological surveys, can be useful tools for helping understand the geological evolution of karst areas.
In order to enhance the reconstruction of the structural setting in a gypsum karst area (Vena del Gesso, Romagna Apennines), a detailed analysis has been carried out on hypogeal data. Structural features (faults, fractures, tectonic foliations, bedding) have been mapped in the ”Grotta del Re Tiberio” cave, in the nearby gypsum quarry tunnels and open pit benches. Five fracture systems and six fault systems have been identified. The fault systems have been further analyzed through stereographic projections and geometric-kinematic evaluations in order to reconstruct the relative chronology of these structures. This analysis led to the detection of two deformation phases.
The results permitted linking of the hypogeal data with the surface data both at a local and regional scale. At the local scale, fracture data collected in the underground have been compared with previous authors' surface data coming from the quarry area. The two data sets show a very good correspondence, as every underground fracture system matches with one of the surface fracture system. Moreover, in the cave, a larger number of fractures belonging to each system could be mapped. At the regional scale, the two deformation phases detected can be integrated in the structural setting of the study area, thereby enhancing the tectonic interpretation of the area (*e.g.,* structures belonging to a new deformation phase, not reported before, have been identified underground).
The structural detailed hypogeal survey has, thus, provided very useful data, both by integrating the existing information and revealing new data not detected at the surface. In particular, some small structures (*e.g.,* displacement markers and short fractures) are better preserved in the hypogeal environment than on the surface where the outcropping gypsum is more exposed to dissolution and recrystallization.
The hypogeal geological survey, therefore, can be considered a powerful tool for integrating the surface and log data in order to enhance the reconstruction of the deformational history and to get a three-dimensional model of the bedrock in karst areas.

Keywords: hypogeal geological survey • structural analysis • gypsum karst • Vena del Gesso • Grotta del Re Tiberio

*E-mail: alice.ghiselli@gmail.com

1. Introduction

Karst systems are natural windows to the underground; therefore, speleology, combined with geological surveys, can be useful tools for helping understand the geological evolution of karst areas. In this paper, the results of mesoscale structural analysis of hypogeal data are shown.

The study area is the Re Tiberio karst system and the old exploited tunnels of the nearby gypsum quarry, located in the "Vena del Gesso" (Romagna Apennines, Italy). The "Vena del Gesso" is a spectacular gypsum ridge, up to 30 km long, standing out on the smooth landscape of the Western-Romagna foothills [1]. The wide gypsum outcrop provides a unique view to the primary evaporites related to the Messinian Salinity Crisis of the Mediterranean [2]. The gypsum surface exposure to dissolution and recrystallization, though, sometimes prevents the detection of mesoscale, both primary and secondary features. Therefore the presence of natural caves and quarry tunnels can provide an important contribution to the interpretation of the geological evolution of the area.

Moreover, the evaporitic rocks within sedimentary sequences play an important role in localizing deformation, especially in thrust tectonics, implying that their strength is generally lower than that of other rock [3]. Therefore, as gypsum can register deformation features that other rocks do not show, its study can provide further information with respect to the contiguous rocks. Gypsum, in fact, accommodates strain by brittle and plastic deformation mechanisms, developing Riedel-like faults with plastic foliations and crystallographic preferred orientation as the other rocks [4], but at lower temperatures and strain rates.

2. Structural setting

The study area is part of the "Vena del Gesso", a shallow water evaporitic succession belonging to the Romagna Apennines, a section of the Northern Apennines bounded from the Sillaro valley to the northwest and the Marecchia valley to the southeast (Fig. 1).

2.1. The Romagna Apennines

The Romagna Apennines are part of the northeast-verging Northern Apennine, a fold-and-thrust belt developed since the Late Cretaceous, as a result of convergence between the European plate and the Adria microplate [5–7]. During its eastward migration, the Apennines thrust front incorporated progressively younger siliciclastic deposits [8] leading to the development of "piggy-back" and thrust-top basins above the moving thrust sheets (*e.g.* [1, 6, 9]).

The Romagna Apennines represent the lowest structural unit of the Apennine orogenic wedge [9]. This tectonic unit mainly is constituted by the Marnoso-Arenacea formation turbiditic complex (Langhian to Tortonian) [10]. The Marnoso Arenacea is detached at the level of the Lower Miocene sediments from its Early Tertiary and Mesozoic carbonate succession along a flat basal thrust and is deformed by fault-propagation folds, sometimes forming imbricate structures [11–13], resulting in a regional northeast-verging duplex [1] with NW-SE trending thrusts. To the west of the Sillaro valley, the Romagna Apennine structural unit is covered by the Ligurian nappe (Fig. 2), a mélange formed during the Late Cretaceous Alpine compressional phases and subsequently (during the Apennine orogeny, in post-Oligocene times) thrust over the Adria plate [14, 15]. To the northeast the Marnoso Arenacea grades to Messinian to Pleistocene deposits assembled in a monocline dipping NNE [9] (Figs 1, 2).

In the central part, the Romagna Apennines are split into two sectors by the Forli line, a deformational zone characterized by reverse NNW-SSE trending faults [9]. This tectonic feature played a primary role in the geologic evolution of the area, at least since the late Tortonian [8] (Fig. 2).

The sedimentation of the Romagna fore-deep succession was strongly influenced by syn-sedimentary activity of thrust sheets and by the pre-sedimentary basin morphology (*e.g.* [1, 9, 10, 16]). In-sequence and out-of-sequence activation of these syn-tectonic thrusts led to the development of thrust-top basins among which the Vena del Gesso basin is one of the most representative [1].

2.2. The "Vena del Gesso" basin

The Vena del Gesso is a shallow water evaporitic succession deposited in a small thrust-top basin developed starting from Late Tortonian-Early Messinian during the thrust front propagation of the Apennine orogenic wedge towards the foreland [8]. To the north and to the east the northwest-southeast trending Vena del Gesso basin is bounded by the Riolo Anticline, a buried anticline plunging westward below the Ligurian nappe along the Sillaro valley [9] (Fig. 2).

The gypsum succession is completely detached at its base and is characterized by a southwestern sense of shear (backwards with respect to the Apennine foreland vergence) [1] and a NNE general dip. Moreover, reverse faults, both transverse and sub-parallel to the northwest-southeast trending Vena del Gesso ridge, repeatedly doubled the evaporites [17]. The Colombacci Formation, whose base has been dated at 5.50+/-0.2 Ma (Late Messinian) [18], sealed the backthrusts, thus con-

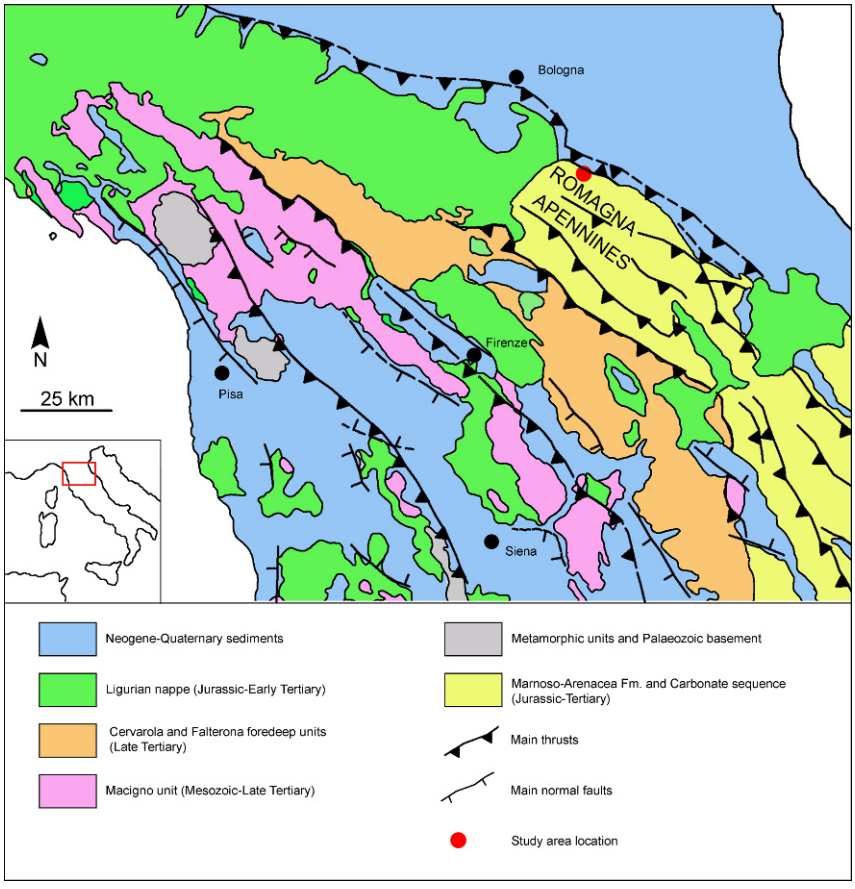

Figure 1. Geological setting of the Northern Apennines. The Romagna Apennines and the study area location are indicated (modified after [1]).

straining their timing of activity.

Afterwards, the Vena del Gesso area was dissected by near vertical, northeast-southwest trending faults, accommodating the last stages of deformation [17].

2.3. The study area

The study area is located near Borgo Rivola village in the central part of the Vena del Gesso and belongs to the southern and western slopes of Monte Tondo (Fig. 3). The main structure outcropping in the area is the Scarabelli Fault, a near vertical, WNW-ESE trending fault [19]. The geometry and kinematics of this fault are not clear as it is represented by an intensely fractured wide zone, rather than by a deformation band with exposed fault planes. This fault is interpreted by Forti *et al.* [19] as a NNE dipping, listric, SSW verging intra-messinian backthrust, in accordance with the Montanari *et al.* [1] model, accounting for a southwest vergence of the Vena del Gesso thrusting. Roveri *et al.* [9] interpret it as a deformational feature mainly related to gravity processes associated with the presence of a Tortonian, SW-dipping paleo-surface that triggered large-scale slope instability phenomena, thus promoting the collapse and accumulation of huge gypsum slabs, which was then tilted by the Pliocene to Holocene deformation phase (Fig. 16 in [9]).

Another fault in the study area is reported by Forti *et al.* [19] called "Sassoletroso Nord" (SLN in Fig. 3), a direct, SSW-dipping, low angle fault associated with the "Sassoletroso Sud" (SLS in Fig. 3), a reverse S-dipping fault with a higher angle. Both faults, visible in the open pit quarry fences, are referred to as an extensive post-lower Pliocene deformation phase [19].

3. Stratigraphical setting

The Romagna Apennines middle-Miocene to Pliocene sedimentary succession is divided into four formations [20]:

1. The Marnoso-Arenacea Formation (Langhian-Messinian) is constituted by deep-water siliciclastic turbidites mainly derived from alpine sources [9].

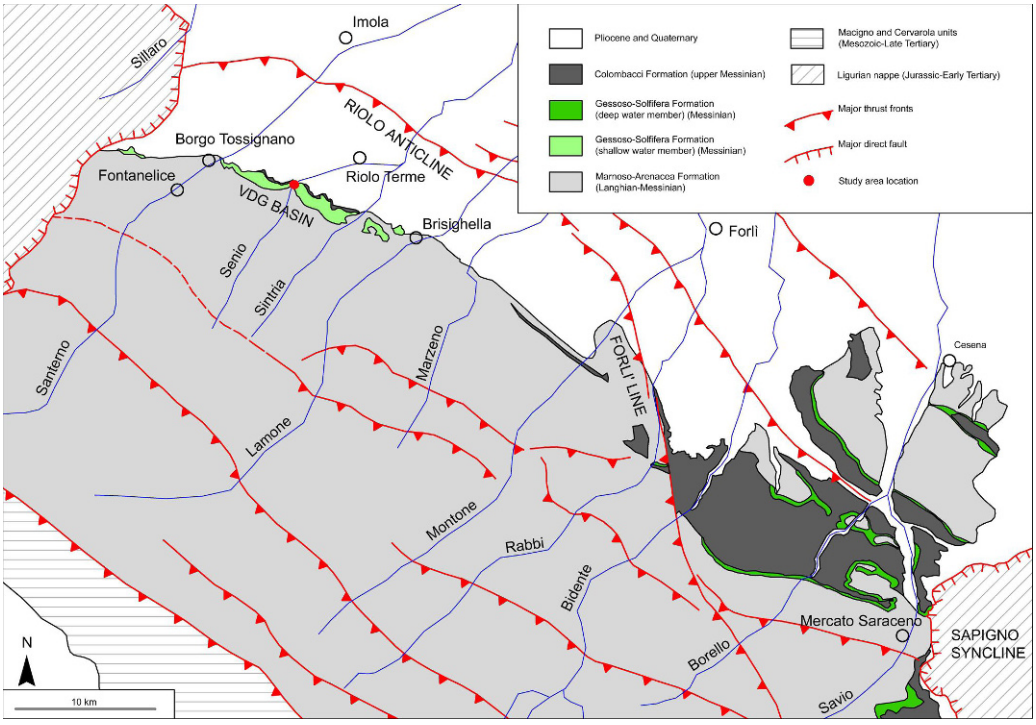

Figure 2. Geological setting of the Romagna Apennines. The Vena del Gesso (VDG) basin location and the main structural features are indicated (modified after [9]).

The upper part of the Marnoso-Arenacea formation is covered by a thin layer characterized by cyclically interbedded organic-rich laminites and mudstones, informally referred to as "euxinic shales" (Late Tortonian–Early Messinian) [9]. The "euxinic shales" record the paleoceanographic changes forerunning the Messinian salinity crisis [9].

2. The Gessoso-Solfifera Formation (Messinian) is represented by both primary and clastic resedimented evaporites with interbedded organic-rich shales, deposited during the evaporitic and post-evaporitic stages of the Messinian salinity crisis [9]. The complete succession is divided into 15-16 major beds, each representing one evaporitic cycle, mainly constituted by macro-crystalline gypsum, from a few to 30 meters thick, with a thickness trend reducing from the base to the top [17]. The complete evaporitic cycle is constituted by six *facies* [21] starting with euxinic mudstones, overlapped by a layer of stromatolitic and clastic carbonates and gypsum, passing to layers of autochthonous selenite and, towards the top, to clastic and reworked selenite [17].

3. The Colombacci Formation (Late Messinian), constituted by siliciclastic sediments, are derived from Apenninic sources, and deposited in brackish or freshwater basins during the last phases of the Messinian salinity crisis [9].

4. The Argille Azzurre Formation (Early Pliocene), made up of mudstones, was deposited in a deep marine enviroment, locally including conglomerates and sandstones bodies and small, isolated carbonate platforms [9].

In the study area only the Gessoso-Solfifera Formation crops out. The Marnoso Arenacea formation outcrops to the south, while the Colombacci Formation to the north-east. The sedimentary succession general dip direction is NNE, the dipping varies from 23° to 55° [19].

4. Karst system geomorphology

In the Monte Tondo area two karst systems with a total extension of about 10 km are present [22]. The "Grotta del Re Tiberio" cave is the drainage gallery of the system constituted by the "Abisso Cinquanta", "Abisso Mezzano", "Tre Anelli", "Inghiottitojo del Re Tiberio" caves (system A in Fig. 4). To the other karst system belong the "Buca

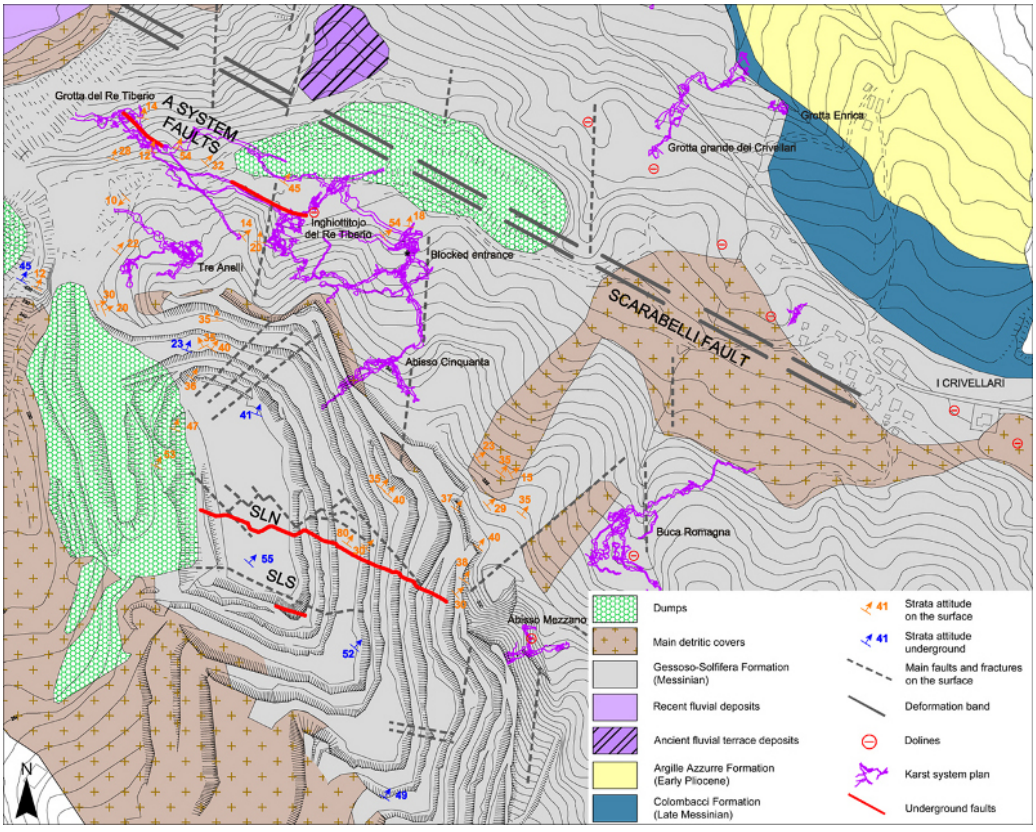

Figure 3. Geological map of the Monte Tondo area; the red traces indicate the A system, the Sassoletroso Nord (SLN) and Sassoletroso Sud (SLS) faults detected underground (modified after [19]).

Romagna", "Grotta grande dei Crivellari", "Grotta Enrica", "Grotta uno di ca' Boschetti", "Grotta due di ca' Boschetti" and "Risorgente a nord-ovest di ca' Boschetti" caves (system B in Fig. 4).

The total extension of the Re Tiberio system caves, not all physically connected to each other, is about 6300 m with a difference in height of 223 m [23]. The system's general orientation is NW-SE, even if there are many labyrinth-like strokes and some galleries with a SW-NE trend [23].

The "Grotta del Re Tiberio" cave develops mostly horizontally, with four overlapping levels of galleries connected by short vertical pits (Fig. 5). Galleries are numerous, mostly horizontal, seldom inclined, with different morphologies: gorge-like galleries, flat vault galleries, and square-shaped galleries. Pits show different morphologies as well: stepped pits, bell-shaped pits, and square-shaped pits. Chambers are rare and generally show morphologies due to collapses; their width and length are greater than their height; metric clast deposits are abundant on the floor. Some small chambers formed at a junction of passages, while others are constituted by the enlarged base of joined pits.

5. Methodology

5.1. Structural survey

Faults and bedding data have been collected in the "Grotta del Re Tiberio" cave, in the nearby gypsum quarry tunnels and benches (Fig. 6). Fractures data have been collected in the "Grotta del Re Tiberio" cave only. In the galleries and on the benches, in fact, the quarry workings have generated a large number of artificial fractures deleting or deflecting the natural ones. Moreover, a good fracture data set collection on the quarry fences, through a terrestrial 3d laser scanner method and traditional survey, had been recently carried out by Blois and Berry [24], for stability conditions analysis.

Faults and their kinematics have been recognized by stratigraphic and structural criteria. If the fault cuts a stratigraphic surface visible both in the footwall and in the hanging wall, its displacement has been inferred from the new geometric relationships (stratigraphic criteria). In all other cases the fault movement has been inferred from displacement markers: calcite fibres, gypsum fibres or striae

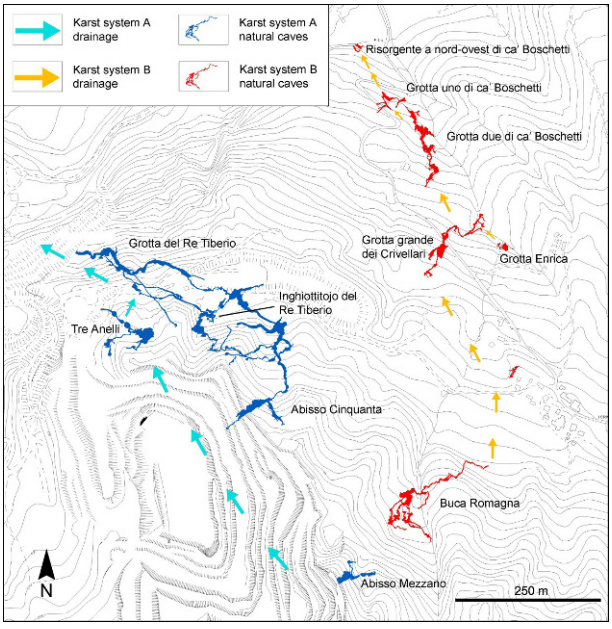

Figure 4. The two Monte Tondo karst systems; the first one (system A) is constituted by "Grotta del Re Tiberio", "Abisso Cinquanta", "Abisso Mezzano", "Tre Anelli", "Inghiottitojo del Re Tiberio" caves, the second one (system B) by "Grotta grande dei Crivellari", "Grotta Enrica", "Grotta uno di ca' Boschetti", "Grotta due di ca' Boschetti" and "Risorgente a nord-ovest di ca' Boschetti" caves (modified after [19]).

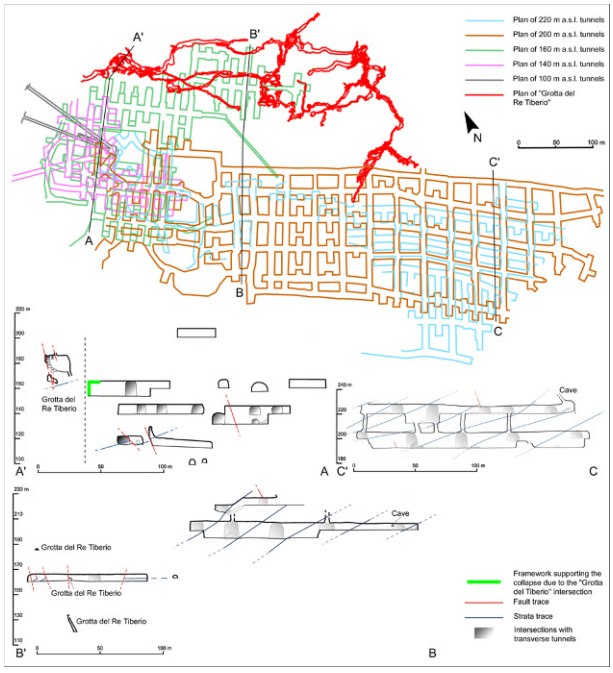

Figure 6. Geometric relationships between the "Grotta del Re Tiberio" cave and the quarry tunnels; plan view and sections. The faults traces, the bedding traces and the intersections with caves are indicated in the sections.

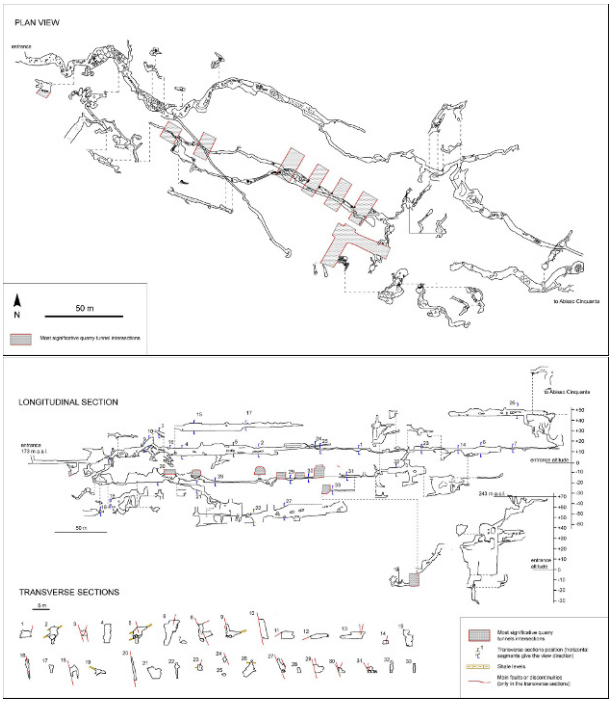

Figure 5. Topographic map and section of the "Grotta del Re Tiberio" cave (modified after [22]).

(structural criteria). Moreover, the presence of variously thick cataclastic deformation bands, sometimes associated with tectonic foliations, permitted the more important and continuous faults to be identified.

For each fault, fault plane dip direction and dip, displacement marker dip direction and dip, pitch, fault length, fault gap, filling material (as cataclasites or mineralizations) have been collected.

For each fracture, fracture plane dip direction and dip, opening, trace length, filling material, and trend have been collected. The data of fractures shorter than 20 cm have not been collected.

5.2. Structural data analysis

After separating faults and fractures data, underground and surface data have been analyzed together.

In order to reconstruct the deformation history of the study area, at first, faults have been grouped on the basis of their dipping and kinematic in six fault systems (Fig. 10). Afterwards, the paleostress field orientation has been calculated for each fault system [27] (Fig. 11). Systems with similar paleostress orientation have been then assigned to the same deformation phase. Moreover, the geometric-kinematic relationships between the fault systems belong-

ing to the same deformation phase have been verified using the Riedel model [25–28] (Fig. 7). Unfortunately, few intersection relationships between faults could be observed. Although the underground environment offers a great 3d point of view, the narrow cavities do not permit following of the outcropping structures for all their extension. Therefore the intersection relationships could not be used for reconstructing the relative chronology of the observed structures. The relative chronology of the detected deformation phases could be inferred, though, thanks to the presence of overlapping displacement markers on the same fault planes.

This chronological information has been integrated with the existing structural data, permitting the insertion in the regional tectonic setting.

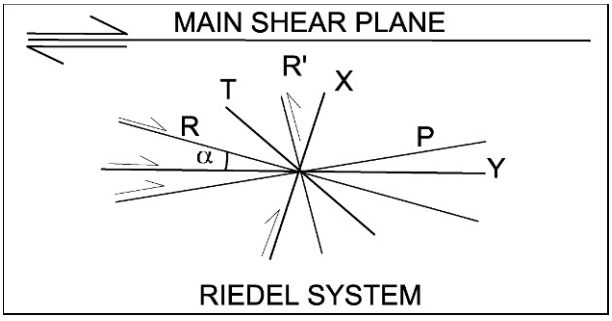

Figure 7. Riedel shear zone geometry.

Fractures data have been analyzed to evaluate their distribution, their compatibility with the fault systems, as well as their relationships with the quarry activity. Fractures due to quarry workings have been separated from the natural ones thanks to their recent aspect, the absence of filling, and their irregular trend. In order to minimize the effects of the quarry workings on the structural setting interpretation of the study area, only the natural fractures have been analyzed. Moreover, as the fractures data set is rather scattered, detecting the fractures dip systems needed further analysis. Using the trace length as the discriminant parameter, its values have been plotted on a cumulative frequency curve (Fig. 8). The two inflexion points of the curve (corresponding to X values 0,3 and 1 of Fig. 8) represent the limits of three length classes (classes 2, 3 and 4). In addition, another length class (class 1, Fig. 8) has been created in order to compare our data with the Blois and Berry [24] dataset. In fact as Blois and Berry [24] analyzed fractures longer than 1 m only, all the fractures shorter than 1 m have been grouped in the first class. Moreover, the central length class (class 3), highlighted by the cumulative frequency curve, represents most of the fractures, thus grouping fractures with very scattered dip values. Therefore, for helping the detection of dip systems, the fractures length values have been plotted on a frequency histogram too, that highlighted a log-normal distribution (Fig. 9). The relative frequency maximum at the X value 0.7, followed by a clear frequency drop (Fig. 9), helped with the detection of two subclasses (subclasses 3a and 3b).

This analysis permitted five fracture systems to be detected. These results have been then compared with previous authors' surface data coming from the quarry area [24].

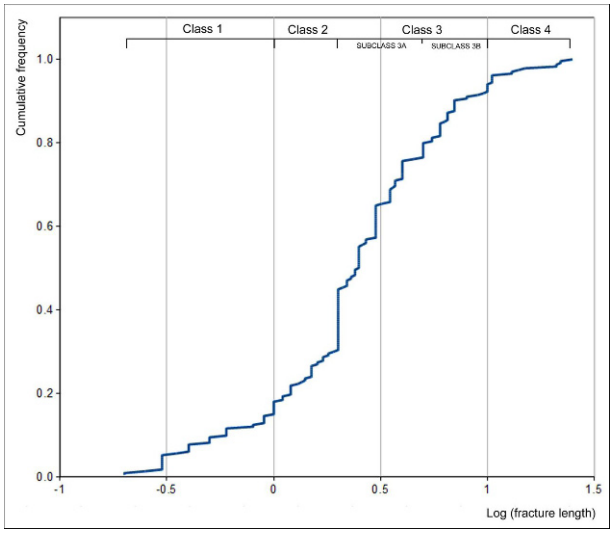

Figure 8. Trace length cumulative frequency curve. On the X axis the Log_{10} of the length values, on the Y axis the cumulative frequency (values are normalized).

6. Meso-structural data and analysis

6.1. Faults

The 139 faults detected have been grouped into six fault systems: two present in the natural cave only, three present in the quarry tunnels and on the benches, and one present both in the cave and in the quarry. Faults with unknown kinematics have been assigned to each system on the basis of their geometric compatibility and/or contiguity with other known faults. Seven faults could not be assigned to any of the fault systems identified.

A system (in the cave only): left-lateral faults with dip direction SW and dip 82°-90° (Fig. 10a);

B system (in the cave only): right-lateral faults with dip direction SSW and dip 85°-88° (Fig. 10b);

C system (both in the cave and in the quarry): direct fault

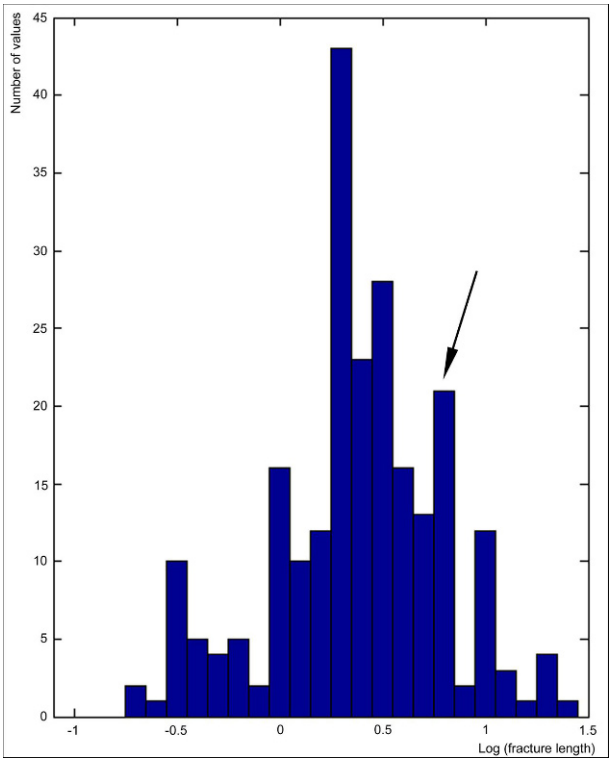

Figure 9. Trace length frequency histogram. On the X axis the Log_{10} of the length values, on the Y axis the numbers of values. Note the Log-normal distribution with the maximum value around 2,5 m. The arrow indicates the relative frequency maximum at the X value 0.7, followed by a clear frequency drop, helping with the detection of the subclasses 3a and 3b.

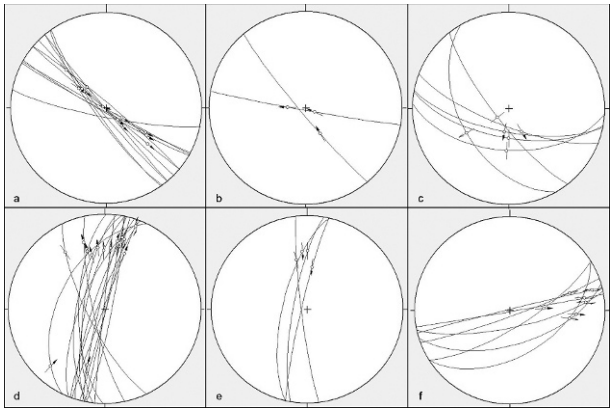

Figure 10. Equal area Schmidt projection, lower hemisphere, of fault planes (arrows indicate the sense of movement on fault planes). a) A system faults, b) B system faults, c) C system faults, d) D system faults, e) E system faults, f) F system faults.

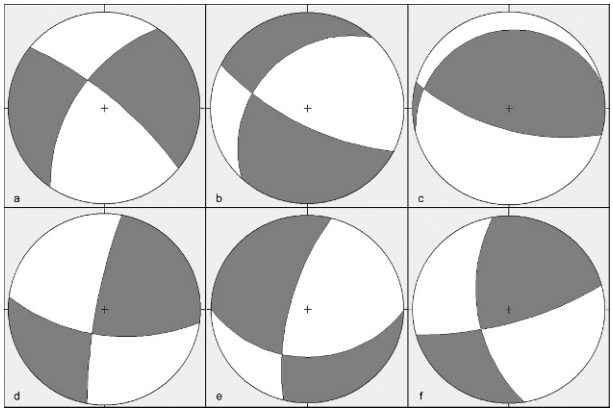

Figure 11. Equal area Schmidt projection, lower hemisphere, of the paleostress compressional and extensional fields of each fault system. a) A system paleostress, b) B system paleostress, c) C system paleostress, d) D system paleostress, e) E system paleostress, f) F system paleostress.

with dip direction SSW and dip 70°-78° (Fig. 10c);

D system (in the quarry only): right-lateral faults with dip direction W and dip 50°-90° (Fig. 10d);

E system (in the quarry only): left-lateral faults with dip direction W and dip 70°-85° (Fig. 10e);

F system (in the quarry only): left-lateral faults with dip direction SE and dip 50°-90° (Fig. 10f).

The fault systems' kinematic compatibility has been evaluated first by calculating the paleostress orientation for each fault system. Paleostress dihedra, which show the compressional and extensional fields, have been plotted (Fig. 11). Considering the extension of the two fields, the fault systems have been grouped into two paleostress groups: the A, C, D, F systems in one group and the B, E systems in another. This grouping then has been verified using the Riedel model, detecting two deformation phases: deformation phase 1 (named "d1 phase") and deformation phase 2 (named "d2 phase").

d1 phase (Figs 12a, 13a, 14b)

The A and D system faults are the most common in the cave and in the quarry tunnels respectively. They belong to the same deformation phase (d1 phase), as their paleostress orientations are similar (cfr. Fig. 11a and Fig. 11d). Moreover, considering the A system as the main shear plane and the D system as the X fault system of the Riedel model, their kinematic compatibility is verified (Fig. 14a). The C system belongs to the same deformation phase (cfr. Fig. 11c and Figs 11a,d) and can be interpreted as the R fault system according to the Riedel model (Fig. 14a). Though the F system paleostress orientation is similar to the D system one, its geometry and kinematics are not compatible with the Riedel-like model of the d1 phase. Therefore the F system has not been

assigned to the d1 phase.

d2 phase (Figs. 12b, 13b, 14b)

The B system paleostress orientation is not compatible with the d1 phase faults (cfr. Fig. 11b and Fig. 11a). Moreover, some B system structures are represented by the same fault planes of the A system, with another series of displacement markers overlapped to the A system ones. Therefore the B system does not belong to the same deformation phase of the A system and has been assigned to another deformation phase called the d2 phase.

The E system paleostress orientation is similar to the B system. According to the Riedel model, it represents the R' fault system of the d2 phase, while the E system is the main shear plane (Fig. 14b).

The F system is not compatible with any of the two phases; therefore, it belongs to another, not identified, deformation phase.

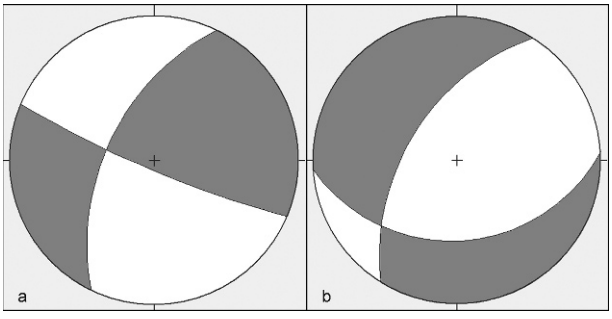

Figure 12. Equal area Schmidt projection, lower hemisphere, of the paleostress compressional and extensional fields of the two deformation phases. a) d1 phase paleostress, b) d2 phase paleostress.

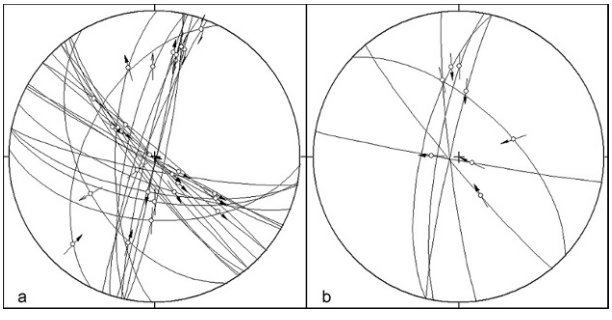

Figure 13. Equal area Schmidt projection, lower hemisphere, of fault planes (arrows indicates the sense of movement on faults planes). a) d1 phase fault planes, b) d2 phase fault planes.

The compressional-extensional field dihedra (Figs 12a,b) of two deformation phases show the different orientations of the two phases' paleostress.

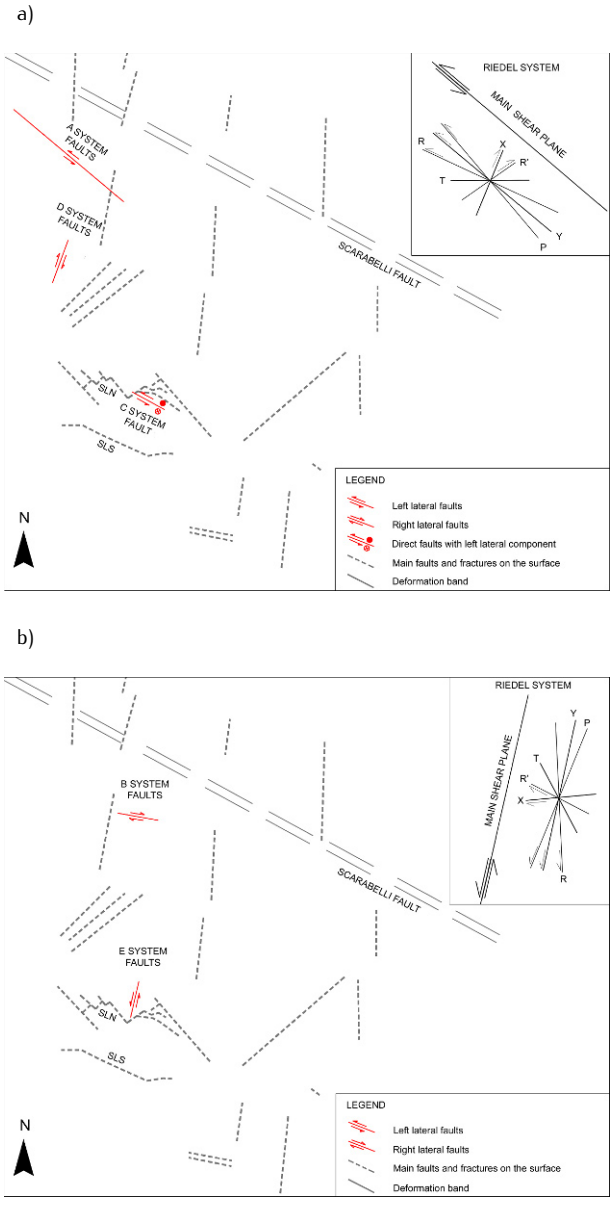

Figure 14. Riedel-like model of the two deformation phases; the traces of fault systems are indicated; SLN=Sassoletroso Nord Fault, SLS= Sassoletroso Sud Fault; faults and fractures data on the surface from [19]. a) d1 phase Riedel-like model, b) d2 phase Riedel-like model.

The stereographic projections of the faults belonging to the two phases (Figs 13a,b) highlight the abundance of the d1 phase structures with respect to the d2 phases.

The two phases' relative chronology has been reconstructed on the basis of the geometric relationships between structures belonging to different deformation phases. Both in the cave and in the quarry tunnels, it was possible to observe the relationships between the two

deformation phases directly. Some examples of overlapping displacement markers, in fact, have been detected. In particular in the "Grotta del Re Tiberio" cave, two series of overlapping displacement markers testify two different movements along the same SW-dipping fault plane (Fig. 15): the displacement markers "a" indicate a left-lateral movement and belong to the A system, while the displacement markers "b" indicate a right-lateral movement and belong to the B system. As the "b" markers are placed upon the "a" markers, the B system faults have been interpreted as following the A system ones.

Another clear and significant example has been observed in the tunnels, where two other series of overlapping displacement markers testify two different movements along the same W-dipping fault plane: the displacement markers "d" indicate a right-lateral movement and belong to the D system, while the displacement markers "e" indicate a left-lateral movement and belong to the E system. As the "e" markers are placed upon the "d" markers, the E system faults have been interpreted as following the D system ones.

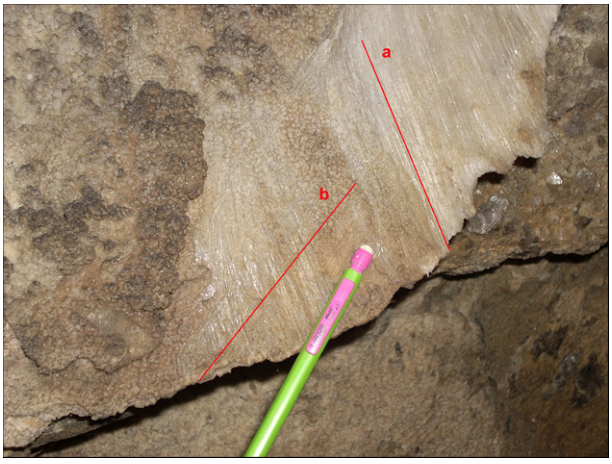

Figure 15. B system displacement markers overlapping the A system ones on the same SW-dipping fault plane in the "Grotta del Re Tiberio" cave; "a" indicates the A system left-lateral movement, "b" indicates the B system right-lateral movement.

6.2. Fractures

Natural fractures data have been grouped into five trace length classes chosen on the basis of their trace length distribution highlighted by the cumulative frequency curve (Fig. 8) and the frequency histogram (Fig. 9).

1) class 1 – length 0.20 m to 1 m (Fig. 16a, maximum value around 249°/59°);

2) class 2 – length 1 m to 2 m (Fig. 16b, maximum value around 16°/54°);

3) class 3 – length 2 m to 5 m (Fig. 16c, maximum value around 111°/59°);

4) class 4 - length 5 m to 10 m (Fig. 16d, maximum value around 232°/69°);

5) class 5 – length greater than 10 m (Fig. 16e, maximum value around 227°/84°).

The stereographic projections show the fracture systems present in each length class and the values around which most of the fractures concentrate. The length classes grouping helps in detecting the following fracture systems.

G system: dip direction SW, dip 50° to 90°, fractures prevailing in the classes 1, 4 and 5;

H system: dip direction ESE, dip around 69°, fractures prevailing in the class 3;

I system: dip direction NNE, dip around 54°, fractures prevailing in the class 2.

The stereographic projection of all the natural fractures shows the maximum concentration of fractures around the value 45°/16° (Fig. 16g). This datum shows a good correspondence with the bedding dipping (Fig. 16f), as most of the fractures overlap with the bedding. It is possible, therefore, to detect another fracture system: the L system.

L system: dip direction NE, dip around 16°. This system is present in each length class and in the fractures due to quarry workings as well (Fig. 16h). This distribution shows the influence of bedding on fracture development.

The stereographic projection of all the natural fractures (Fig. 16g) highlights another iso-density cloud of the poles that can be observed in the class length projections. This datum permits detection of another fracture system: the M system.

M system: dip direction NNW, dip around 70°.

This fracture analysis led to the identification of five main systems (Fig. 16g, Tab. 1); some of them could be associated with the stratigraphic or structural features detected in the area. In particular:

- the G system fractures are parallel to the faults belonging to the A, B or C systems, and therefore could be associated with any of the three systems;
- the L system fractures are parallel to the gypsum bedding, therefore their development has likely been controlled by the bedding orientation.

7. Discussion

7.1. Deformation chronology

The mesostructural analysis permitted the detection of two deformation phases: the d1 phase, including A, C and D

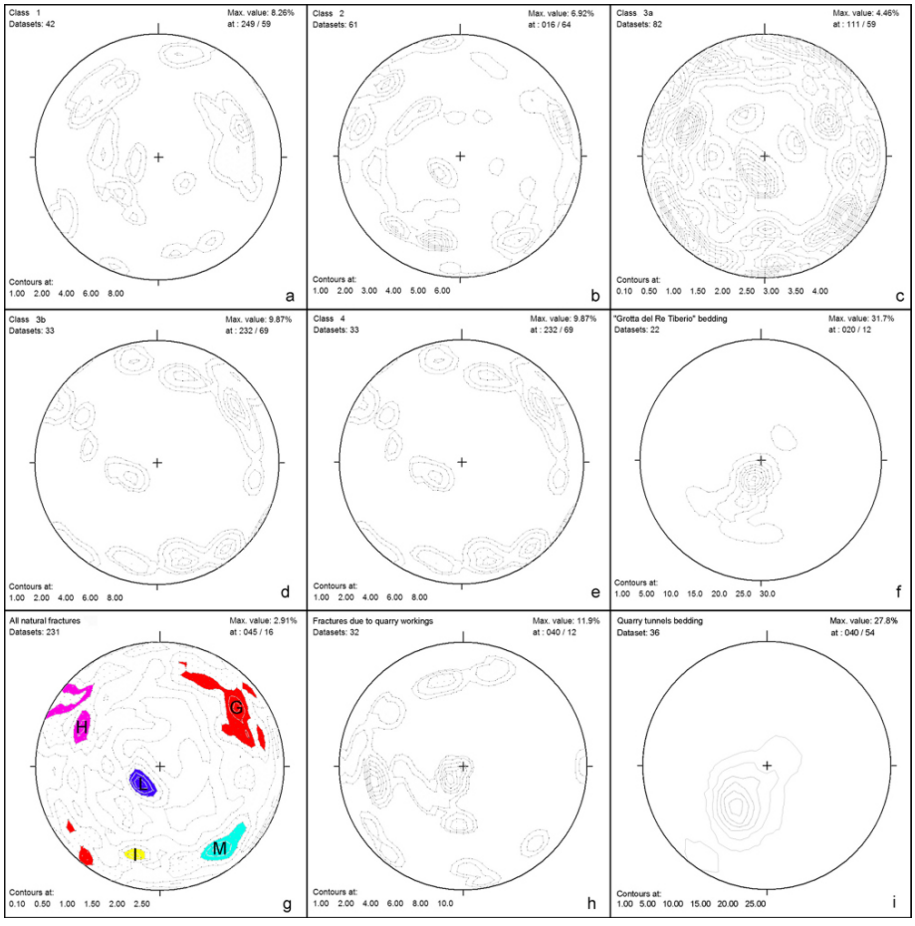

Figure 16. Equal area Schmidt projection, lower hemisphere, of poles of fracture planes and bedding; iso-density lines are shown; iso-density contours (in percentage) are indicated in the lower-left corner. a) class 1 fractures poles, b) class 2 fractures poles, c) subclass 3a fractures poles, d) subclass 3b fractures poles, e) class 4 fracture poles, f) "Grotta del Re Tiberio" cave bedding values poles, g) all natural fractures poles (the fracture systems are indicated), h) fractures due to quarry workings poles, i) quarry tunnels bedding poles.

Table 1. Summary table of the faults and fractures data. System name, medium dip direction, medium dip angle, outcrop enviroment and notes are indicated.

	phase	system	dip direction	dip angle	localization	kinematic
faults	d1	A	SW	82°-90°	cave only	left-lateral faults
		C	SSW	70°-78°	cave and quarry	direct faults
		D	W	50°-90°	quarry only	right-lateral faults
	d2	B	SSW	85°-88°	cave only	right-lateral faults
		E	W	70°-85°	quarry only	left-lateral faults
		F	SE	50°-90°	quarry only	left-lateral faults
	system		**dip direction**	**dip angle**	**localization**	**notes**
fractures	G		SW	50°-90°	cave	compatible with the A, B or C systems
	H		ESE	69°	cave	
	I		NNE	54°	cave	
	L		NE	16°	cave	parallel to bedding
	M		NNW	70°	cave	

systems, and the d2 phase, including B and E systems (Tab. 1).

The Sassoletroso Nord fault reported by Forti *et al.* [19] belongs to the C system. In fact, it has been detected both in the quarry tunnels and on the benches (the Sassoletroso faults traces are indicated in Fig. 3: the grey lines represent the fault traces on the surface, from Forti *et al.* [19], the red lines represent the fault traces, detected in the quarry tunnels). The C system faults, therefore, can be referred to as the same post-lower Pliocene deformation phase of the Sassoletroso Nord and Sassoletroso Sud faults (Fig. 3).

The A system faults have the same trend of the Scarabelli fault (Fig. 3), even if their kinematic is different: though the Scarabelli Fault kinematic and orientation are not clear (see the structural setting-study area paragraph) it can be interpreted as a reverse fault, while the A system faults are left-lateral faults. As no direct data on the Scarabelli Fault kinematic exist, it is not possible to find a clear relationship between the Scarabelli Fault and the A system fault. However, a hypothesis can be formulated: the A system faults could have developed as reverse faults, together with the Scarabelli Fault, during the intra-messinian deformation phase [19] and then could have been later reactivated as left-lateral faults. Anyhow, as the A system faults belong to the same deformation phase of the C system faults they can be dated back to the post-lower Pliocene deformation phase of Forti *et al.* [19].

Therefore the d1 phase can be dated back to a period post-lower Pliocene.

The structural analysis permitted reconstruction of the relative chronology of the d1 and d2 phases through the overlapping of displacement markers belonging to the two phases. As the E system faults have been interpreted as following the D system ones, the d2 phase is more recent than the d1 phase. Therefore the d2 phase can be dated back to a period following the post-lower Pliocene. This phase can be related to the lower-middle Pliocene-Quaternary phase described by Marabini and Vai [17], as the authors mention the development of lateral faults with geometry similar to that of the E-system faults. They do not specify if these faults are left or right lateral, though, therefore it is not possible to certainly date back the d2 phase to the lower-middle Pliocene-Quaternary. Further studies would permit to clarification of the age of the d2 phase.

7.2. Integration of existing surface data

Faults: As discussed in the previous paragraphs, the structural data collection and the following analysis permitted six fault systems to be grouped into two deformation phases to be identified. In the study area, all the d2 phase, and some of the d1 phase, structures were not reported by previous authors. In particular, the A and B system faults have been interpreted as reactivated intra-messinian apenninic faults, with a strike-slip kinematic. Previous authors [17, 19] mentioned the reactivation during the post-lower Pliocene phase of intra-messinian structures, but only for anti-apenninic faults (*i. e.* faults that transverse to the apenninic thrusts' main direction). Moreover, in the whole area, a large number of faults were not reported before on the surface and could be mapped in the underground.

Fractures: Fractures data of the "Grotta del Re Tiberio" cave have been compared with surface data of Blois and Berry [24], coming from the quarry area. The two data sets show a very good correspondence: the G system corresponds to the group 1 (average dip 225°/78°) of Blois and Berry [24], the H system to the group 2 (average dip 128°/69°), the I system to the group 5 (average dip 38°/62°), the L system to the group 4 (average dip 35°/36°) even if the dip angle is lower in the cave than on the surface, and the M system to the group 3 (average dip 315°/76°). Therefore, all the fracture groups detected on the surface in the quarry have been identified in the cave as well. Moreover, in the cave a larger number of fractures have been mapped thanks to the better outcropping condition. The hypogeal data set, though, shows a greater dispersion with respect to the surface data set (*cfr.* Fig. 16g with Fig. 8 in [24]).

The differences between the two data sets can be interpreted as follows. Regarding the greater data dispersion in the cave, the Blois and Berry [24] data set is less scattered both because of their choice of collecting data for fractures more than one meter long only, and because of the better outcropping condition in the cave which permitted us to identify a larger number of fractures. Even if the Blois and Berry [24] data set does not include fractures shorter than one meter, the two data sets are still comparable. In fact, when removing the fractures belonging to the class 1 (from 0.20 m to 1 m long), the analysis results do not change as the shorter fractures do not highlight a particular fracture system not shown by other fracture classes.

Regarding the fracture dip variation between the L system and the group 4 of Blois and Berry [24], the L system is directly controlled by rock bedding, which could be due to a regional variation of the strata geometry. In fact, the dip of gypsum bedding in the tunnels is higher than in the "Grotta del Re Tiberio" cave (*cfr.* Fig. 16f and Fig. 16i) . The two data sets show an increase of the bedding medium dip angle from 16° in the cave (to the NW) to 36° in the quarry tunnels (to the SE) (Fig. 3). As the tunnels are

closer to the quarry "amphitheatre", sometimes even underneath, the steeper bedding could have controlled the dip of the group 4 fractures of Blois and Berry [24] on the benches. This variation should explain the difference between the medium dip angle of L system and the group 4.

8. Conclusions

The structural data collection in the "Grotta del Re Tiberio" cave, in the tunnels and on the benches of the quarry nearby, together with the following analysis, permitted six fault systems, grouped into two deformation phases and five fracture systems to be identified (Tab. 1). The interpretation of the results permitted a link wth the hypogeal data, with the surface data both at a local and a regional scale.

At the local scale, fractures data collected in the underground have been related to the surface data collected in the quarry area by Blois and Berry [24]. The two data sets show a very good correspondence, as every underground fracture system matches with one of the surface fracture system. Differences in the two data sets are due to the variation of strata dip that controls the development of one of the fracture systems. The greater dispersion of the fracture data in the cave, with respect to the surface, is due both to the underground collection of small fractures and to the better outcropping condition in the cave, permitting identification of a larger number of fractures. In fact, small structures, as fractures, are better preserved in the hypogeal environment than on the surface, where the outcropping gypsum is more exposed to dissolution and recrystallization that can delete some features.

At the regional scale, the two deformation phases detected can be integrated in the structural setting of the study area. The d1 phase corresponds to the post-lower Pliocene phase of Forti *et al.* [19]. Besides the dip-slip faulting pointed out by previous authors, the presence in the study area of lateral faults, kinematically compatible with the dip-slip faults, permitted the detection of strike-slip faulting active during the post-lower Pliocene phase.

The d2 phase, not reported by previous authors in the study area, could be related to the lower-middle Pliocene-Quaternary phase described by Marabini and Vai [17] in the surrounding area.

Therefore, the hypogeal geological survey in the study area permitted many new faults and one new deformation phase to be identified in the study area. In particular, strike-slip faulting, which probably reactivated some intramessinian faults, has been detected and related to the post-lower Pliocene phase. Moreover, a new deformation phase (the d2 phase) has been identified in the study area and probably related to the lower-middle Pliocene-Quaternary phase of the regional setting.

The hypogeal geological survey can be, therefore, considered a powerful tool for integrating the surface and log data. In fact, the underground data provide continuous information about the geometry of geological bodies under the topographic surface. Thus, the hypogeal geological survey can be used for enhancing the reconstruction of the deformational history and for getting at a three-dimensional model of the bedrock in karst areas. In addition, hypogeal survey can be considered as an alternative direct method of underground investigation for mining engineering matters.

Acknowledgements

This study was financially supported by the Monte Tondo quarry property Saint-Gobain PPC Italia S.p.A., since scientific research is part of the company's sustainable development program.

Moreover, we would like to thank Dr. Fabrizio Felletti, Dr. Michele Zucali and an anonymous reviewer for their precious suggestions.

References

[1] Montanari D., del Ventisette C., Bonini M., Sani F., Passive-roof thrusting in the Messinian Vena del Gesso basin (Northern Apennines, Italy): constraints from field data and analogue models. Geol. J. , 2007, 42, 455-476

[2] Selli R., Il Messiniano Mayer-Eymar 1867. Proposta di un Neostratotipo. Giornale di Geologia, 1960, 28, 1-33

[3] Barberini V., Burlini L., Rutter E. H., Dapiaggi M., High-strain deformation tests on natural gypsum aggregates in torsion. In: Bruhn D., Burlini L. (eds.), High-Strain Zones: Structure and Physical Properties. Geological Society of London Special Publications, London, 2005, 245, 277-290

[4] Zucali M., Barberini V., Chateigner D., Ouladdiaf B., Lutterotti L., Brittle plus plastic deformation of gypsum aggregates experimentally deformed in torsion to high strains: quantitative microstructural and texture analysis from optical and diffraction data. Geol. Soc. Spec. Publ., 2010, 332, 79-98

[5] Boccaletti M., Calamita F., Deiana G., Gelati R., Massari F., Moratti G. et al., Migrating foredeep-thrust belt system in the Northern Apennines and

southern Alps. Palaeogeogr., Palaeoecol., 1990, 77, 3-14

[6] Principi G., Treves B, Il Sistema Corso-Appennino come prisma d'accrezione. Riflessi sul problema generale del limite Alpi-Appennini. Memorie della Societá Geologica d'Italia, 1984, 28, 529-576

[7] Malinverno A., Ryan WBF, Extension in the Tyrrhenian Sea and shortening in the Apennines as a result of arc migration driven by sinking of the lithosphere. Tectonics, 1986, 5, 227-246

[8] Ricci Lucchi F., The Oligocene to Holocene foreland basins of the Northern Apennines. In: Allen P.A., Homewood P. (eds.), Foreland basins. International Association of Sedimentologists Special Publication, 1986, 8, 105-139

[9] Roveri M., Manzi V., Ricci Lucchi F., Rogledi S., Sedimentary and tectonic evolution of the Vena del Gesso basin (Northern Apennines, Italy): implications for the onset of the Messinian salinity crisis. Geol. Soc. Am. Bull., 2003, 115, 4, 387-405

[10] Ricci Lucchi F., Miocene paleogeography and basin analysis in the Periadriatic Apennines. In: Squyres, C.H. (ed.), Geology of Italy. Petroleum Exploration Society of Lybia, Tripoli, 1975, 2, 129-236

[11] Capozzi R., Landuzzi A., Negri A., Vai G.B., Stili deformativi ed evoluzione tettonica della successione neogenica romagnola. Studi Geologici Camerti Special Volume, 1991, 1, 261-278

[12] Benini A., Farabegoli E., Martelli L., Stratigrafia e paleogeografia del Gruppo di S. Sofia (alto Appennino Forlivese). Memorie Descrittive della Carta Geologica d'Italia,1991, 46, 231-243

[13] Farabegoli E., Benini A., Martelli L., Onorevoli G., Severi P., Geologia dell'Appennino Romagnolo da Campigna a Cesenatico. Memorie Descrittive della Carta Geologica d'Italia, 1991, 46, 165-184

[14] Kligfield R.,The Northern Apennines as a collisional orogen. Am. J. Sci., 1979, 279, 676-691

[15] Boccaletti M., Elter P., Guazzone G., Plate tectonics models for the development of Western Alps and Northern Apennines. Nature, 1971, 234, 108-111

[16] Ricci Lucchi F., The Oligocene to Recent foreland basins of the Northern Apennines. In: Allen P.A., Homewood P. (eds.), Foreland Basins. International Association of Sedimentologists Special Publications, 1986, 8, 105-139

[17] Marabini S., Vai G.B., Analisi di facies e macrotettonica della Vena del Gesso in Romagna. B. Soc. Geol. Ital., 1985, 104, 21-42

[18] Krijgsman W, Hilgen FJ, Marabini S, Vai GB., New paleomagnetic and cyclostratigraphic age constraints on the Messinian of the Northern Apennines (Vena del Gesso Basin, Italy). Memorie della Societá Geologica Italiana, 1999, 54, 25-33

[19] Forti P., Marabini S., Vai G.B., Convenzione con il Comune di Riolo Terme sullo studio geologico, idrogeologico e carsico della porzione della Vena del Gesso romagnola interessata dalla cava di gesso di Borgo Rivola. Relazione Preliminare, Bologna, 1997 http://www.venadelgesso.org/testi/cave/fortimarabinivai/cava5.htm

[20] Vai G.B., A field trip guide to the Romagna Apennine geology, the Lamone valley. In: De Giuli C., Vai G.B. (eds.), Fossil vertebrates in the Lamone valley, Romagna Apennines, International Workshop: Continental Faunas at the Mio-Pliocene Boundary, Field Trip Guidebook, Litografica, Faenza, 1988, 7-37

[21] Vai G.B., Ricci Lucchi F., Algal crusts, autochtonous and clastic gypsum in a cannibalistic evaporite basin: a case history from the Messinian of Northern Apennines. Sedimentology, 1977, 24, 211-244

[22] Ercolani M., Lucci P., Sansavini B.,L'esplorazione dei sistemi carsici del Re Tiberio e dei Crivellari (Vena del Gesso Romagnola) e la salvaguardia dell'area di Monte Tondo interessata dall'attivitá di cava. Istituto Italiano di Speleologia – Memoria, 2003, 16, 2, 147-157

[23] Bentini L., I principali sistemi carsici della Vena del Vesso romagnola e il loro condizionamento strutturale. In: Gruppo speleologico bolognese (ed.), Proceedings of the 19th National Congress of Speleology, Bologna, 2003, 27-31

[24] Blois L., Berry B., Measurements to characterize discontinuities of quarry faces of chalk "Monte Tondo" in Riolo Terme (Italy) trough terrestrial 3d laser scanning method and to compare them at survey techniques data traditional. Electronic Journal of Geotechnical Engineering, 2008, 13, 1-29

[25] Riedel W., Zur mechanik geologischer Brucherscheinungen. Zentralblatt fur Mineralogie, Geologie und Palaeontologie, 1929, B, 354-368

[26] Tchalenko J.S., Similarities between shear zones of different magnitudes. Geol. Soc. Am. Bull., 81, 1625-1639

[27] Nicolas A., Principles of rock deformation. Reidel Publishing Company, Dordrecht, 1987

[28] Gapais D., Cobbold P. R., Bourgeois O., Rouby D., de Urreiztieta M., Tectonic significance of fault-slip data. J. Struct. Geol., 2000, 22, 881-888